The Journal of Physiology

Molecular mechanisms of Slo2 K^+ channel closure

M. Hunter Giese[1], Alison Gardner[1], Angela Hansen[1] and Michael C. Sanguinetti[1,2]

[1]*Nora Eccles Harrison Cardiovascular Research & Training Institute*
[2]*Department of Internal Medicine, Division of Cardiovascular Medicine, University of Utah, Salt Lake City, UT, USA*

Key points

- Intracellular Na^+-activated Slo2 potassium channels are in a closed state under normal physiological conditions, although their mechanisms of ion permeation gating are not well understood.
- A cryo-electron microscopy structure of Slo2.2 suggests that the ion permeation pathway of these channels is closed by a single constriction of the inner pore formed by the criss-crossing of the cytoplasmic ends of the S6 segments (the S6 bundle crossing) at a conserved Met residue.
- Functional characterization of mutant Slo2 channels suggests that hydrophobic interactions between Leu residues in the upper region of the S6 segments contribute to stabilizing the inner pore in a non-conducting state.
- Mutation of the conserved Met residues in the S6 segments to the negatively-charged Glu did not induce constitutive opening of Slo2.1 or Slo2.2, suggesting that ion permeation of Slo2 channels is not predominantly gated by the S6 bundle crossing.

Abstract Large conductance K^+-selective Slo2 channels are in a closed state unless activated by elevated $[Na^+]_i$. Our previous studies suggested that the pore helix/selectivity filter serves as the activation gate in Slo2 channels. In the present study, we evaluated two other potential mechanisms for stabilization of Slo2 channels in a closed state: (1) dewetting and collapse of the inner pore (hydrophobic gating) and (2) constriction of the inner pore by tight criss-crossing of the cytoplasmic ends of the S6 α-helical segments. Slo2 channels contain two conserved Leu residues in each of the four S6 segments that line the inner pore region nearest the bottom of the selectivity filter. To evaluate the potential role of these residues in hydrophobic gating, Leu267 and Leu270 in human Slo2.1 were each replaced by 15 different residues. The relative conductance of mutant channels was highly dependent on hydrophilicity and volume of the amino acid substituted for Leu267 and was maximal with L267H. Consistent with their combined role in hydrophobic gating, replacement of both Leu residues with the isosteric but polar residue Asn (L267N/L270N) stabilized channels in a fully open state. In a recent cryo-electron microscopy structure of chicken Slo2.2, the ion permeation pathway of the channel is closed by a constriction of the inner pore formed by criss-crossing of the S6 segments at a conserved Met. Inconsistent with the S6 segment crossing forming the activation gate, replacement of the homologous Met residues in human Slo2.1 or Slo2.2 with the negatively-charged Glu did not induce constitutive channel opening.

(Received 29 July 2016; accepted after revision 20 September 2016; first published online 28 September 2016)
Corresponding author M. C. Sanguinetti: Nora Eccles Harrison Cardiovascular Research & Training Institute, University of Utah, Salt Lake City, UT 84112 USA. Email: m.sanguinetti@utah.edu

Abbreviations EM, electron microscopy; $I_{c\text{-}rel}$, relative magnitude of constitutive Slo2 channel current; $I_{Slo2.1}$, Slo2.1 channel current; $I_{Slo2.2}$, Slo2.2 channel current; I–V_t, current–voltage; MD, molecular dynamics; MPS, membrane propensity scale; NFA, niflumic acid; PH, pore helix; SF, selectivity filter; V_h, holding potential; V_t, test voltage; WT, wild-type.

 DOI: 10.1113/JP273225

Introduction

Slo2.1 (Slick, KCNT2) and Slo2.2 (Slack, KCNT1) are large conductance, K^+ selective channels that are normally in a closed state unless activated by an increase in intracellular Na^+ and Cl^- ions (Bhattacharjee *et al.* 2003, Yuan *et al.* 2003). Slo2 channels are widely expressed throughout the mammalian brain (Bhattacharjee *et al.* 2002, Bhattacharjee *et al.* 2005, Rizzi *et al.* 2016) where they have been proposed to have several functions in neurons, including stabilization of the resting membrane potential, adaptation of firing pattern and generation of slow after-hyperpolarizations (Yang *et al.* 2007, Gao *et al.* 2008, Zhang *et al.* 2010). In rodents, Slo2 channels exhibit differential tissue expression. Slo2.2 channels are widely expressed in the mammalian brain, with especially high expression in the brainstem, deep cerebellar nuclei, olfactory bulb and dorsal root ganglia (Bhattacharjee *et al.* 2002, Rizzi *et al.* 2016). Slo2.1 channel expression not only partially overlaps with Slo2.2 (e.g. olfactory bulb), but also is preferentially expressed in hippocampal regions CA1–CA3, the hypothalamus, cortical layers II – IV (Bhattacharjee *et al.* 2005) and the heart (Bhattacharjee *et al.* 2003). Knockout in mice of Slo2.1 and Slo2.2, either singly or together, results in an unexpectedly mild phenotype. Slo2.2 knockout mice exhibit a brief exaggerated itch response and mice lacking both Slo2 channels have a mildly increased pain sensation (Martinez-Espinosa *et al.* 2015). Knockout of Slo2.2 by another group indicated increased hypersensitivity in models of neuropathic pain, although not in models of inflammatory or acute nociceptive pain (Lu *et al.* 2015). Mutations in Slo2.2 have also been implicated in several types of early onset epilepsies in humans (Barcia *et al.* 2012, Heron *et al.* 2012, Vanderver *et al.* 2014). To date, mutations in Slo2.1 have not been associated with human disease.

Slo2 channels can be activated by close coupling with channels that conduct persistent Na^+ current in neurons (Hage and Salkoff, 2012) or in response to elevated $[Na^+]_i$ that can occur during ischaemia in the heart (Kameyama *et al.* 1984). When Slo2 channels are heterologously expressed in oocytes or mammalian cell lines, the channels remain closed unless activated by elevated $[Na^+]_i$, especially when accompanied by an increase in $[Cl^-]_i$ (Bhattacharjee *et al.* 2003). Slo2 channels can also be highly activated by extracellular application of niflumic acid (NFA) or other fenamates (Dai *et al.* 2010, Garg and Sanguinetti, 2012).

In a typical Kv channel, ion permeation is controlled by a coupling of intramembrane displacement of the primary voltage sensors (S4 segments) to an activation gate formed by the S6 bundle crossing, a criss-crossing of the S6 α-helical segments that line the inner pore (Long *et al.* 2005). According to this widely accepted model of K^+ channel gating, channels are closed when the S6 bundle crossing forms an aperture that is too narrow to allow diffusion of hydrated K^+ ions. The structural basis of Slo2 channel gating is not as well defined. Activation of Slo2.1 channels exhibits very weak voltage dependence (effective valence, $z = 0.48$ e) that is not altered even after neutralization of all the charged residues in the S4 segments of the voltage sensor domain (Dai *et al.* 2010), suggesting that Slo2 channels are primarily ligand-gated. Based on results from scanning mutagenesis of the pore domain, we previously proposed that the selectivity filter (SF) performs as the activation gate in Slo2.1 (Garg *et al.* 2013) in a manner similar to that previously described for other channels, including Slo1 (Wilkens and Aldrich, 2006, Thompson and Begenisich, 2012), $K_{Ca}2.2$ (Bruening-Wright *et al.* 2007), $K_{Ca}3.1$ (Klein *et al.* 2007, Garneau *et al.* 2009, Garneau *et al.* 2014), MthK (Posson *et al.* 2013) and K2P channels (Zilberberg *et al.* 2001, Piechotta *et al.* 2011). Mutation to Ala of either Pro271 or Glu275 in the S6 segment locked the Slo2.1 channel in a non-conducting state, presumably by narrowing of the central cavity when a kink in S6 is removed (P271A mutation) or electrostatic repulsion between Glu residues is eliminated (E275A mutation). Mutation of the aromatic residue (Phe240) located between the pore helix (PH) and the SF to a polar residue (e.g. F240C) induced constitutive channel opening (Garg *et al.* 2013). Mutation of the transmembrane segment S5 residue Leu209 to Glu or Gln induced maximal channel activation, as did the combined mutation to Ala of all three hydrophobic S5 residues predicted to be adjacent to Phe240, suggesting that hydrophobic interactions between residues in S5 and the C-terminal end of the PH stabilize Slo2.1 channels in a closed state (Suzuki *et al.* 2016). Together, these findings suggested a model for Slo2.1 channel gating that involves dynamic, hydrophobic coupling between Phe240 in the PH and Leu209 in S5 (Fig. 1) (Garg *et al.* 2013, Suzuki *et al.* 2016). However, our model of channel activation based on functional analysis of mutant Slo2.1 channels does not agree with a recent cryo-electron microscopy (EM) structure of the chicken Slo2.2 channel where the S6 bundle crossing at Met333 constricts the inner pore to an aperture with a radius estimated to be too small (4–6 Å) to allow permeation of a hydrated K^+ ion (Hite *et al.* 2015). Human Slo2.1 and Slo2.2 channel subunits also contain a Met residue in the same position in the S6 segment as Met333 in chicken Slo2.2.

Another mechanism of K^+ channel gating has been proposed. All atom molecular dynamics (MD) simulations of ion permeation through the Kv1.2 channel indicated that hydrophobic gating can mediate pore closure at negative transmembrane potentials (Jensen *et al.* 2010). Specifically, the central cavity can undergo a stochastic liquid–vapour transition (Aryal *et al.* 2015) from an open, ion conducting state to a collapsed, non-conducting state by molecular scale dewetting (dehydration) and this

process was facilitated when K^+ ions were not bound to the sites in the SF nearest the central cavity (Jensen *et al.* 2010). Hydrophobic gating of the MscS mechanosensitive bacterial channel is mediated by the side chains of two Leu residues that face the central cavity; rotation of these residues leads to opening and closing of the central pore (Wang *et al.* 2008). The K2P channel TWIK-1 also has two Leu residues that line the inner pore and replacement of these residues with the isosteric but polar residue Asp increased channel open probability (Aryal *et al.* 2014). Slo2.1 channels also have two Leu residues (Leu267 and Leu270) that are located nearest the SF in the S6 segment of each subunit (Fig. 1*A*) and line the cavity of the inner pore (Fig. 1*B*).

In the present study, we use a site-directed mutagenesis approach to evaluate the potential role of hydrophobic gating in the activation of Slo2 channels. We also provide a functional test of the prediction that, based on the cryo-EM structure of Slo2.2, the ion permeation pathway of Slo2 channels is closed by a constriction of the inner pore formed by the S6 bundle crossing.

Methods

Ethical approval

Procedures used to harvest oocytes from adult female *Xenopus laevis* were approved by the University of Utah Institutional Animal Care and Use Committee (IACUC). Frogs were purchased from Xenopus 1 (Dexter Township, MI, USA).

Frog surgery and oocyte isolation

IACUC policy number P001 'Oocyte harvesting in *Xenopus laevis*' was consulted as a guide to the procedures described below and elsewhere. *Xenopus laevis* frogs were anaesthetized by immersion in 0.2% tricaine methane sulphonate (MS-222, adjusted to pH 7 with Na bicarbonate) for ~30 min. When the frog was fully anaesthetized, as assessed by the lack of a response to toe pinch, the abdomen was swabbed with betadine solution before making an abdominal incision. Using a sterile technique, a few ovarian lobes were removed and the incision was sutured closed. The frog was allowed to fully recover for at least 1 month before oocyte harvest was performed again. After the third surgery, frogs were killed by cervical dislocation when fully anaesthetized with MS-222. Our methods comply with the AVMA Guidelines for the Euthanasia of Animals and the animal ethics checklist outlined in (Grundy, 2015). Freshly isolated stage 4 or 5 oocytes were incubated at 17 °C in Barth's saline solution that contained (in mM): 88 NaCl, 1 KCl, 0.41 $CaCl_2$, 0.33 $Ca(NO_3)_2$, 1 $MgSO_4$, 2.4 $NaHCO_3$, 10 Hepes and 1 pyruvate, plus gentamycin (50 mg l^{-1}), amikacin (50 mg l^{-1}) and ciprofloxacin (25 mg l^{-1}). The pH of Barth's solution was adjusted to 7.4 with NaOH.

Molecular biology

Human Slo2.1 (*KCNT2*) cDNA in pTRACER was kindly provided by L. Kaczmarek (Yale University, New Haven, CT, USA) and subcloned into psGEM as described

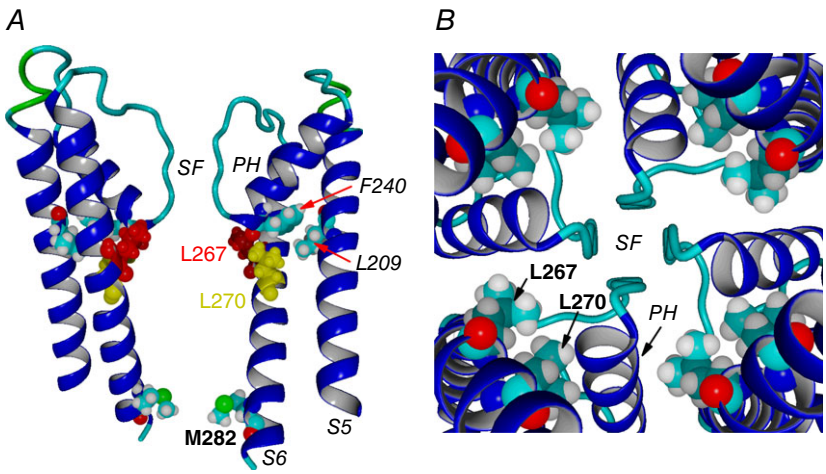

Figure 1. Structure of the Slo2 channel pore region
A, structure of the S5–S6 region of two diagonal chicken Slo2.2 subunits (Protein Data Bank code: 5A6E). In one subunit, the PH, selectivity filter (SF), S5 and S6 segments and select residues with numbering that corresponds to amino acid position in the human Slo2.1 subunit are labelled. The three residues probed by site-directed mutagenesis in the present study (Leu267, Leu270, Met282) are highlighted in colored or bold text. Also shown are Leu209 in the S5 segment in close proximity to Phe240 located at the base of the PH. The side chain of Met282 residues face directly towards the inner cavity. *B*, structure of the pore region of a homotetrameric Slo2.2 channel viewed from the cytoplasmic side. Leu267 and Leu270 residues from all four subunits line the cavity of the inner pore. Images were prepared using YASARA (Krieger *et al.* 2002; Krieger *et al.* 2009).

previously (Dai *et al.* 2010). Human Slo2.2 (*KCNT1 variant 1*) cDNA in the pCR-XL-TOPO vector was obtained from Open Biosystems (Thermo Fisher Scientific Inc., Waltham, MA, USA). A *Mlu*I restriction site was introduced into the 5′ end, and the cDNA was excised from the vector using *Mlu*I and *Xho*I and sub-cloned into the pUNIV vector (Addgene, Cambridge, MA, USA). Point mutations were introduced into wild-type (WT) Slo2.1 or Slo2.2 channels using the QuikChange site-directed mutagenesis kit (Agilent Technologies, Santa Clara, CA, USA). Plasmid DNA was linearized with *Sfi*I (Slo2.1) or *Xba*I (Slo2.2) and cRNA transcribed using the T7 mMessage mMachine RNA kit (Thermo Fisher Scientific Inc.).

Electrophysiology

Xenopus laevis oocytes were injected with a cRNA quantity that was adjusted based on the variable level of expression for the various channel types (0.2–1 ng of cRNA for WT Slo2.1, 1–10 ng of cRNA for mutant Slo2 channels). Oocytes were studied 1–7 days after their injection with cRNA. Oocytes were placed in a 0.3 ml oocyte chamber (RC-1Z; Warner Instruments, Hamden, CT, USA) and superfused at a rate of 1–2 ml min^{-1} with 2 K solution that contained (in mM): 98 NaCl, 2 KCl, 1 $CaCl_2$, 1 $MgCl_2$ and 5 mM Hepes (with the pH adjusted to 7.6 with NaOH). In some experiments, oocytes were bathed in 104 K solution that contained (in mM): 104 KCl, 1 $CaCl_2$, 1 $MgCl_2$ and 5 mM Hepes (with the pH adjusted to 7.6 with KOH). Whole cell currents were recorded at room temperature using standard two-microelectrode voltage-clamp techniques (Stühmer, 1992) and agarose-cushion microelectrodes (Schreibmayer *et al.* 1994) that were fabricated from borosilicate glass (o.d. 1 mm) (TW100F-4; World Precision Instruments, Sarasota, FL, USA) using a Sutter P-97 Flaming/Brown type micropipette puller (Sutter Instruments, Novato, CA, USA). Microelectrodes had a resistance of 0.2–1 MΩ when back-filled with 3 M KCl.

Current-test voltage (I–V_t) relationships were determined by applying 0.5 s pulses to a test voltage (V_t) that ranged from −120 mV to +60 mV, applied in 10 or 20 mV increments with a pulse interval of 6 s. Test pulses were applied from a holding potential (V_h) of −80 or −85 mV. Data acquisition and analysis was performed using a personal computer and a GeneClamp 500 voltage clamp amplifier, Digidata 1322A digitizer and pCLAMP 8.2 software (Molecular Devices, Inc., Sunnyvale, CA, USA).

When expressed in *Xenopus* oocytes, WT Slo2 channels have a very low open probability but can be rapidly activated by an increase in $[NaCl]_i$ or by extracellular application of fenamates such as NFA. In the present study, NFA was used to activate Slo2.1 and Slo2.2 channel currents ($I_{Slo2.1}$ and $I_{Slo2.2}$, respectively). It is important to note that, although the biophysical properties of Slo2.1 current activated by NFA and by elevated $[Na^+]_i$ appear to be similar, it is unknown whether the mode of gating induced by the two ligands is the same. NFA (Sigma-Aldrich, St Louis, MO, USA) was prepared as a 1 M stock solution in dimethyl sulphoxide and stored at −20°C. NFA is poorly soluble in saline solutions and required extensive stirring after correction of pH with NaOH (to pH 7.6) to dissolve the compound for final concentrations of 0.1 to 10 mM. In uninjected oocytes, NFA at concentrations < 3 mM either had no effect or slightly reduced the current magnitude as a result of the blockade of endogenous Ca^{2+}-activated Cl^- currents (White and Aylwin, 1990). Near maximal activation of WT Slo2.1 channels can be achieved by treatment of oocytes with 6 mM NFA (Dai *et al.* 2010, Garg *et al.* 2013). However, 6 mM NFA also increased the magnitude of an unidentified endogenous current in uninjected and cRNA-injected oocytes.

Voltage clamp protocols and data analysis

To quantify the effects of point mutations on the basal activity of channels, the relative magnitude of constitutive Slo2.1 channel current ($I_{c\text{-}rel}$) was estimated as peak $I_{Slo2.1}$ at 0 mV (I_0) under control conditions divided by I_0 in the presence of 6 mM NFA after subtraction of the NFA-activated endogenous current component (NFA I_{0sub}):

$$I_{c\text{-}rel} = \frac{control\ I_0}{NFA\ I_{0sub}}$$

In our previous studies, $I_{c\text{-}rel}$ varied from ∼0.005 for WT Slo2.1 to 1.0 for constitutively fully active mutant channels such as F240C Slo2.1 (Garg *et al.* 2013) and L209E Slo2.1 (Suzuki *et al.* 2016).

To determine whether constitutively active mutant Slo2.1 channels have altered ion selectivity, we determined their relative permeability of Rb^+ and K^+ (P_{Rb^+}/P_{K^+}) under bi-ionic conditions. $I_{Slo2.1}$ was activated by applying steps from −20 to +20 mV in 5 mV increments from a V_h of 0 mV. The reversal potential (E_{rev}) for $I_{Slo2.1}$ was first measured in an oocyte bathed in 104 K solution, and then again after switching to 104 Rb solution that contained (in mM): 104 RbCl, 1 $CaCl_2$, 1 $MgCl_2$ and 5 Hepes (with the pH adjusted to 7.6 with NaOH). P_{Rb^+}/P_{K^+} was calculated from the change in E_{rev} (ΔE_{rev}) according to the Goldman, Hodgkin and Katz equation (Goldman, 1943, Hodgkin and Katz, 1949) as:

$$\frac{P_{Rb^+}}{P_{K^+}} = e^{\Delta E_{rev} F/RT}$$

where F is Faraday's constant, R is the universal gas constant and T is the absolute temperature. For these experiments, WT Slo2.1 channels were activated by 1 mM

NFA or by using recording micropipettes that had a tip resistance of 0.4–1.0 MΩ when filled with a 2 M NaCl solution. Leakage of NaCl out of these pipettes into the oocytes activates $I_{Slo2.1}$ to a maximal extent in 5–10 min (Thomson *et al.* 2015, Suzuki *et al.* 2016). The E_{rev} of constitutively active channels was determined under basal conditions, without activation by NFA or Na^+-loading micropipettes.

Off-line analysis of data was performed using pClamp, version 8 or 9 (Molecular Devices). All data are expressed as the mean ± SEM (n, number of oocytes). All ilustrations were prepared using Origin, version 8.6 (OriginLab, Northampton, MA, USA). To define the concentration–response relationship for NFA, $I_{Slo2.1}$ was measured during repetitive 0.5 s pulses to a V_t of 0 mV from a V_h of −80 or −85 mV. $I_{Slo2.1}$ at the end of the pulse to 0 mV (I_0) was plotted as a function of the $\log_{10}$ of [NFA] and fitted with a logistic equation to determine the EC_{50} and the Hill coefficient (n_H):

$$I_0 = \frac{I_{0min} - I_{0max}}{1 + \left(\frac{[NFA]}{EC_{50}}\right)^{n_H}} + I_{0max}$$

Results

Hydrophobic gating

In MscS and TWIK-1 channels, gating of the ion permeation pathway is mediated by the formation of a reversible hydrophobic barrier involving the side chains of two Leu residues that face the central cavity (Wang *et al.* 2008, Aryal *et al.* 2014, Aryal *et al.* 2015). Replacement of the two Leu residues in TWIK-1 with an isosteric but negatively-charged (Asp) or polar (Asn) residue greatly increased channel open probability, consistent with MD simulations of channel gating that indicated a lack of dewetting of the inner pore in the mutant channels (Aryal *et al.* 2014). We used a similar mutagenesis approach to probe the potential role of two Leu residues (Leu267, Leu270) located in the upper half of the S6 segments, near the SF of Slo2.1 channels (Fig. 1). Slo2.1 channels heterologously expressed in *Xenopus* oocytes have a very low open probability ($I_{c\text{-}rel} = 0.005$) under normal physiological conditions, although they can be highly activated by extracellular application of fenamates such as NFA (Dai *et al.* 2010, Garg and Sanguinetti, 2012, Garg *et al.* 2013). As shown in Fig. 2*A*, 1 mM NFA had no effect on endogenous currents in uninjected oocytes but, at a concentration of 6 mM that induces near maximal activation of WT Slo2.1 channels (Dai *et al.* 2010, Garg and Sanguinetti, 2012, Garg *et al.* 2013), NFA increased outward currents from 50 ± 3 nA to 490 ± 30 nA at 0 mV and from 0.26 ± 0.02 μA to 1.38 ± 0.09 μA at +60 mV (n = 45). Although not insignificant, these effects are small compared to the activation of $I_{Slo2.1}$ by NFA in oocytes after heterologous expression of WT Slo2.1 channels (Fig. 2*B*).

In a homology model based on the chicken Slo2.2 structure, the side-chains of Leu267 and Leu270 in human Slo2.1 line the inner pore cavity of the channel (Fig. 1*B*). Similar to WT Slo2.1, L270N Slo2.1 channels were closed under basal conditions ($I_{c\text{-}rel}$ = 0.003 ± 0.001, n = 5) but markedly activated by 1 and 6 mM NFA (Fig. 2*C*). NFA-activated currents included instantaneous and time-dependent components of activation in response to membrane depolarizations above −20 mV. By contrast, under control conditions, L267N Slo2.1 channels exhibited significant constitutive activity ($I_{c\text{-}rel}$ = 0.64 ± 0.02, n = 5) and conducted outward currents that appeared to activate instantaneously (time independent) at all voltages examined (Fig. 2*D*), although the large capacitance current that precedes the outward ionic current may mask a very fast onset of activation. NFA at 1 mM increased $I_{Slo2.1}$ by ∼30%, whereas 6 mM had no further effect (Fig. 2*D*), indicating an enhanced sensitivity of these mutant channels to activation by the fenamate. Replacement of both Leu residues with Asn induced even greater constitutive activity. L267N/L270N channel currents recorded from oocytes bathed in 2 K solution were instantaneous (time independent) and 1 mM NFA caused only a minimal further activation (Fig. 3*A*). The I–V_t relationships for the double mutant channels before and after treatment of oocytes with 1 and 6 mM NFA are plotted in Fig. 3*B*. $I_{c\text{-}rel}$ of L267N/L270N channels was 0.95 ± 0.02 (n = 10) in oocytes bathed in 2 K solution. We previously noted that the whole cell conductance of those mutant channels (e.g. L209E Slo2.1) exhibiting near maximal constitutive activity (no further activation by NFA) when bathed in 2 K solution was reduced when oocytes were bathed in 104 K solution (Suzuki *et al.* 2016). L267N/L270N Slo2.1 channels were similar in this respect. Although 6 mM NFA had minimal effect on $I_{Slo2.1}$ measured in oocytes bathed in 2 K solution (Fig. 3*B*), currents measured using 104 K solution were enhanced by 25% at −120 mV (Fig. 3*C* and *D*). Thus, in contrast to WT Slo2.1 channels with an $I_{c\text{-}rel}$ of 0.005 (Suzuki *et al.* 2016), L267N/L270N channels are almost fully open under basal conditions. These findings suggest that both Leu residues in each of the S6 segments may participate in forming a reversible hydrophobic barrier to ion permeation. To further characterize the potential role of Leu267 or Leu270 in hydrophobic gating, we next characterized multiple single point mutations of these residues.

Physicochemical properties of Leu267 and Leu270 substitutions that alter constitutive activity of Slo2.1 channels

Leu267 and Leu270 of Slo2.1 were each mutated to several other hydrophobic (Gly, Ala, Val, Ile, Met, Trp, Phe, Tyr), polar (Asn, Gln, Thr, Ser), acidic (Asp, Glu) or basic (His) residues. For each mutant channel, currents were

elicited with 0.5 s depolarizations to 0 mV under control conditions and after achieving a maximal response to 6 mM NFA. The ratio of the two currents was used to define the relative magnitude of constitutive Slo2.1 channel current ($I_{c\text{-}rel}$) for each channel type. The $I_{c\text{-}rel}$ for WT and the 15 different Leu267 and Leu270 Slo2.1 mutant channels is plotted in an ascending order in Fig. 4*A* and *B*, respectively. Note that specific amino acid substitutions of the two Leu residues yielded disparate results. With one notable exception (Asp), $I_{c\text{-}rel}$ was > 0.35 for polar or charged residue substitutions of Leu267. It is unclear why L267D channels exhibit low constitutive activity ($I_{c\text{-}rel} < 0.012$) compared to the other acidic residue substitution, L267E with an $I_{c\text{-}rel}$ of 0.52. Only one mutation (L267H) induced channels to be fully open under basal conditions ($I_{c\text{-}rel} = 1.0$). Similar to Leu267, replacement of Leu270 with His or Gln greatly stabilized the mutant channels in an open state, whereas mutation to other polar residues (e.g. Thr, Ser, Asn) did not. L270D channels were not functional (no measurable currents). L270W channels were almost fully open under basal conditions ($I_{c\text{-}rel} = 0.98 \pm 0.01$, $n = 5$). As shown in Fig. 4*C*, there was no apparent relationship between $I_{c\text{-}rel}$ and a knowledge-based hydrophobicity scale for mammalian α-helical membrane proteins (the

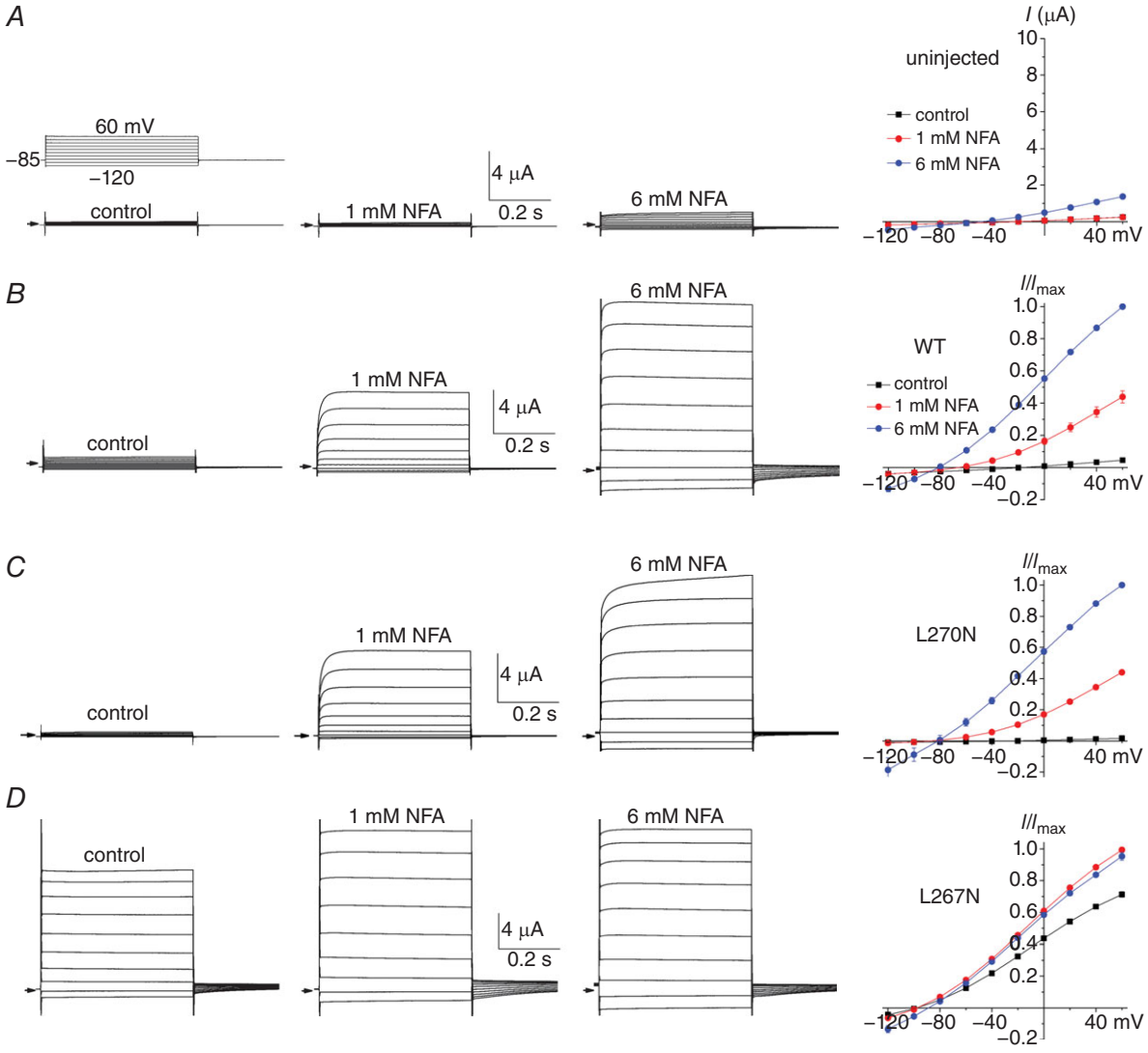

Figure 2. Effects of NFA on L267N and L270N Slo2.1 channel currents
A, voltage pulse protocol, representative current traces recorded from a single uninjected oocyte under control conditions and after treatment with 1 and 6 mM NFA. Right: average I–V_t relationship for 45 uninjected oocytes. *B*, representative current traces and normalized I–V_t relationship for WT Slo2.1 channels ($n = 10$). Right: currents were normalized to the largest currents measured at a V_t of +60 mV. *C*, representative current traces and normalized I–V_t relationship for L270N Slo2.1 channels ($n = 5$). *D*, representative currents and normalized I–V_t relationship for L267N Slo2.1 channels ($n = 5$). In (*C*) and (*D*), the symbol key is the same as that shown in (*B*). All data are the mean ± SEM. Arrows to the left of current traces indicate the zero current level. [Colour figure can be viewed at wileyonlinelibrary.com]

mammalian hydrophobicity scale) (Koehler *et al.* 2009) of the amino acid substitution for either native Leu. To further explore the features that might account for the variable level of constitutive activity of mutant channels, $I_{c\text{-}rel}$ was plotted as a function of two physicochemical properties of the introduced amino acid. Specifically, a contour map was derived by plotting $I_{c\text{-}rel}$ on the *z*-axis (colour-coded), volume of the amino acid when buried in a protein (Richards, 1977) on the *x*-axis and the membrane propensity scale (MPS) value of the substituted amino acids on the *y*-axis (Fig. 4*D* and *E*). MPS is another knowledge-based hydropathy scale that was derived from an extensive transmembrane α-helix database and optimization algorithm (Punta and Maritan, 2003), where a negative value indicates a high membrane propensity. The contour plot for Leu267 substitutions (Fig. 4*D*) indicates that $I_{c\text{-}rel}$ reaches a peak value for amino acid volumes near 160 Å and an MPS value near 0. By contrast, the contour plot for Leu270 substitutions did not reveal a simple interaction of amino acid volume and hydrophobicity that predicted constitutive channel activity (Fig. 4*E*). Replacement of Leu270 with His, Gln or Trp resulted in an $I_{c\text{-}rel} \geq 0.7$. One structural feature common to His, Gln and Trp is the ~4.5 Å spacing between their α carbon and nitrogen atoms (ε^2 N in His), suggesting that interaction with a nearby residue (e.g. Phe240) may be responsible for this large increase in channel open probability.

Constitutively active L267H channels exhibited time independent currents and were not further activated by 1 mM NFA over a wide range of voltage in oocytes bathed in 2 K solution (Fig. 5*A* and *B*). As reported previously (Garg *et al.* 2013, Suzuki *et al.* 2016), partially active mutant Slo2.1 channels are more sensitive to NFA and fully active mutant channels are insensitive to further activation by NFA. However, unlike L267N/L270N Slo2.1 channels (Fig. 3*D*), L267H channels remain fully activated in the presence of high $[K^+]_o$ because even 6 mM NFA did not induce further channel activation (Fig. 5*C* and *D*). L270W channels are also apparently fully open (not further activated by NFA) in oocytes bathed in 2 K solution (Fig. 5*E*), although the whole cell conductance was reduced to half-maximal when currents were recorded from oocytes bathed in 104 K solution (Fig. 5*F*). Thus, the L267H mutation fully stabilizes channels in an open conformation, whereas the open probability of L270W Slo2.1 channels are still partially reduced by elevated $[K^+]_o$.

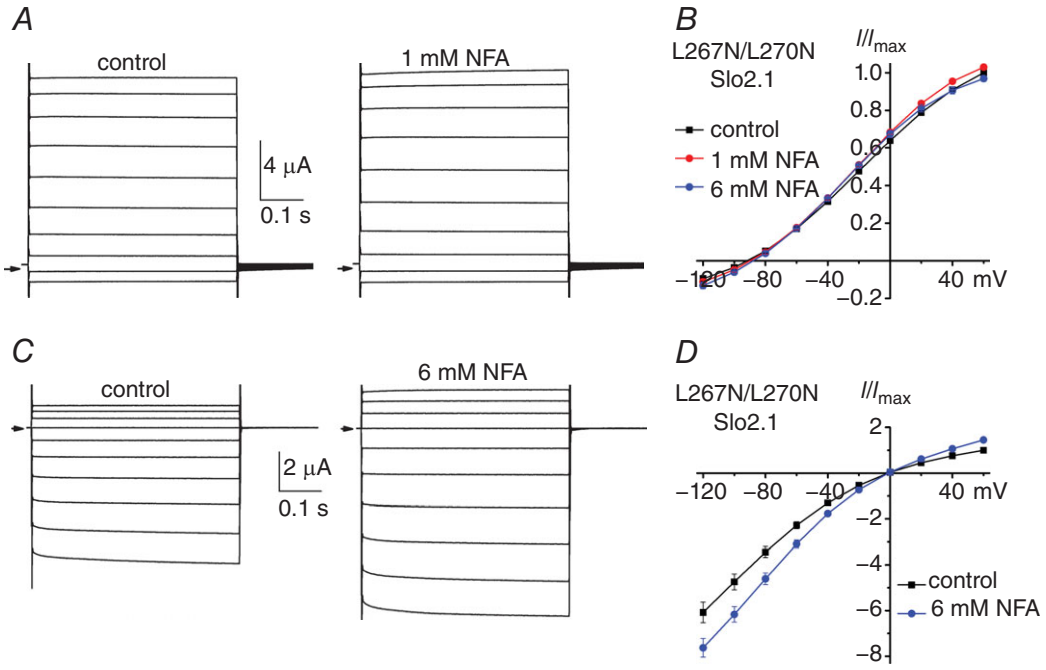

Figure 3. L267N/L270N Slo2.1 channels are constitutively open
A, representative currents recorded from an oocyte bathed in 2 K solution in the absence (control) or presence of 1 mM NFA. Currents were elicited with 0.5 s pulses applied from a V_h of −80 mV to V_t ranging from +60 to −120 mV, applied in −20 mV increments. *B*, I–V_t relationships normalized to control currents measured at +60 mV (2 K bath solution, $n = 10$). *C*, representative currents recorded from an oocyte bathed in 104 K solution in the absence (control) or presence of 6 mM NFA. Currents were elicited with 0.5 s pulses applied from a V_h of 0 mV to V_t ranging from +60 to −120 mV, applied in −20 mV increments. *D*, I–V_t relationships normalized to control currents measured at +60 mV (104 K bath solution, $n = 7$). All data are the mean ± SEM. Arrows to the left of current traces indicate the zero current level. [Colour figure can be viewed at wileyonlinelibrary.com]

Mutations homologous to L267H and L270W in Slo2.1 also stabilize Slo2.2 channels in an open state

The amino acid sequences of human Slo2.1 and Slo2.2 subunits are highly conserved in the transmembrane regions, including the two Leu residues we have characterized in Slo2.1. Leu339 and Leu342 in Slo2.2 correspond to Leu267 and Leu270 in Slo2.1. We introduced the same Leu substitutions in Slo2.2 that produced the greatest change in $I_{c\text{-}rel}$ of Slo2.1. As expected for fully activated channels, L339H $I_{Slo2.2}$ was time independent. However, instead of having no effect, 1 mM NFA reduced current magnitudes by ~45% when oocytes were bathed in 2 K solution (Fig. 6*A* and *B*). This effect was as rapid in onset as the activation of WT channels, suggesting that NFA reduces L339H Slo2.2 channel current by altering gating as opposed to the much slower onset for pore block of Slo2 channels (Garg and Sanguinetti, 2012). Similar to L267H Slo2.1, the I–V_t relationship for L339H $I_{Slo2.2}$ measured in 104 K solution was inwardly rectifying and not altered by 6 mM NFA (Fig. 6*C* and *D*), indicating that this mutation fully stabilized channels in an open state and that the inhibitory effect of NFA was absent in the presence of high $[K^+]_o$. L342W Slo2.2 channels were also highly active under control conditions but, unlike the homologous Slo2.1 mutant, were further activated by 1 mM NFA in both 2 K solution (Fig. 6*E* and *F*) and 6 mM NFA in 104 K solution (Fig. 6*G* and *H*). Even when fully activated by NFA, L342W Slo2.2 channel currents exhibited a slow phase of activation at positive potentials and this was not observed with constitutively active Slo2.1 channels that appear to be instantaneous in onset. In summary, specific Leu substitutions induce constitutive channel opening in both Slo2.1 and Slo2.2 channels.

Ion permeability of constitutively open mutant channels

Several point mutations in the pore domain of Slo2.1 induce partial or maximal constitutive channel opening. In the S6 segment, A278R or E275D mutations activate channels to approximately one-tenth or half-maximal of that which can be achieved by a saturating concentration of NFA or by elevating $[NaCl]_i$ (Garg and Sanguinetti, 2012, Garg *et al.* 2013). In addition to L267W and L270H, three

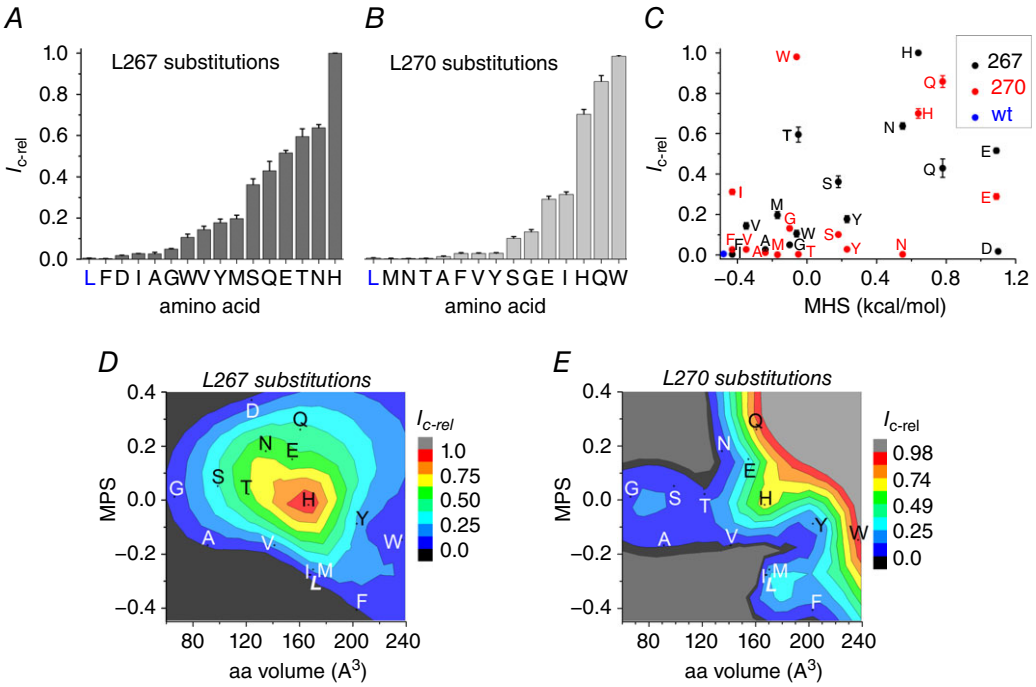

Figure 4. Amino acid substitutions of Leu267 and Leu270 have variable effect on constitutive activity of Slo2.1 channels
A, plot of $I_{c\text{-}rel}$ as a function of the amino acid substituted for Leu267 ($n \geq 5$ for each mutant). Substituted amino acids are indicated by a single letter code. L represents the WT channel. *B*, plot of $I_{c\text{-}rel}$ as a function of the amino acid substituted for Leu270 ($n \geq 5$ for each mutant). *C*, Plot of $I_{c\text{-}rel}$ for mutant channels as a function of the mammalian hydrophobicity scale (MHS) values for introduced amino acids (indicated by single letter code). For both Leu267 and Leu270 mutant channels, there was no significant correlation between $I_{c\text{-}rel}$ and MHS (adjusted r^2 for linear fits are 0.23 and 0.01 for Leu267 and Leu270 data, respectively). All data are the mean ± SEM. *D*, contour plot of $I_{c\text{-}rel}$ (*z*-axis) as a function of the volume (*x*-axis) and the MPS value (*y*-axis) of the residue substituted for Leu267. *E*, contour plot for Leu270 mutant channels. The native Leu residue in both contour plots is indicated in italics.

additional mutations in Slo2.1 (R190E, L209E, F240C) induce maximal channel opening ($I_{c\text{-}rel} = 1.0$) (Dai *et al.* 2010, Garg *et al.* 2013, Suzuki *et al.* 2016). Arg190 is located near the junction of the S4 segment with the S4–S5 linker. Leu209 is located in the S5 segment and homology modelling suggests that the side chain of this residue faces towards Phe240 located at the base of the PH in the same subunit (Fig. 1*A*). $I_{c\text{-}rel}$ is 0.6 for L209T and 1.0 for F240C (Garg *et al.* 2013). If mutations increase channel open probability by affecting the SF gate, then constitutive channel activity might be accompanied by a change in ion selectivity. We examined this possibility by determining the relative permeability of Rb^+ compared to K^+ (P_{Rb^+}/P_{K^+}) for WT and mutant channels. The E_{rev} for $I_{Slo2.1}$ was first measured in oocytes bathed in 104 K solution, and then again after equilibration in 104Rb solution. An example of I–V_t relationships determined under the two ionic conditions is shown for E275D Slo2.1 channels in Fig. 7*A*. In this example, E_{rev} was shifted by −15 mV after switching between 104 K and 104Rb solutions, corresponding to a P_{Rb^+}/P_{K^+} of 0.58 ± 0.003. The P_{Rb^+}/P_{K^+} of other K^+ channels that have been proposed to gate ion permeation at the selectivity filter varies from 0.67 for Slo1 (Blatz and Magleby, 1984) and 0.96 for KCa3 (Grissmer *et al.* 1993). The ΔE_{rev} for WT and all eight of the constitutively active mutant channels is presented in Fig. 7*B*. ΔE_{rev} for WT $I_{Slo2.1}$ was −13.6 ± 0.14 mV when channels were activated with 1 mM NFA and −14.1 ± 0.13 mV when channels were activated by Na^+ loading. With the exceptions of L209E and L270W, the P_{Rb^+}/P_{K^+} for the mutant channels differed significantly ($P < 0.001$) from WT channels (Fig. 7*C*). Compared to WT channels, P_{Rb^+}/P_{K^+} was higher for A278R and L267H channels and lower for E275D, L209T, R190E and F240C

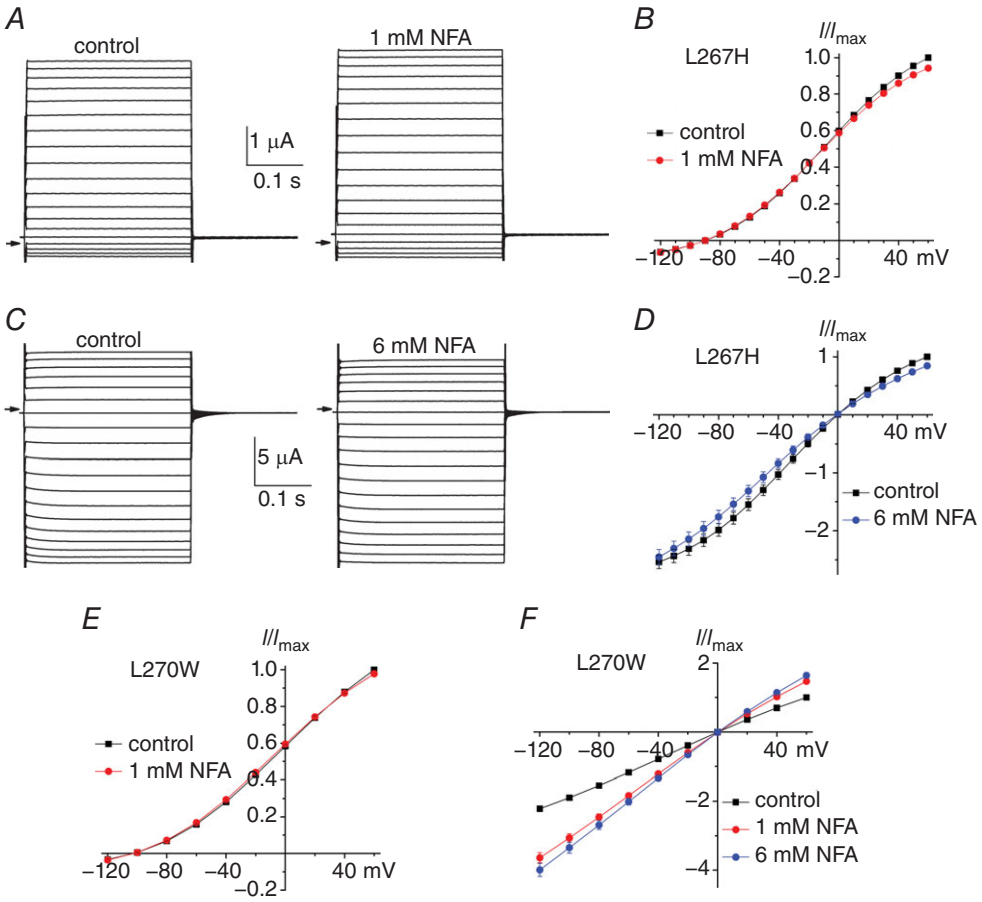

Figure 5. L270W and L267H Slo2.1 channels are constitutively open
A, representative L267H $I_{Slo2.1}$ recorded from a single oocyte bathed in 2 K solution. V_t was varied from +60 to −120 mV, applied in 10 mV steps. *B*, normalized I–V_t relationship for L267H $I_{Slo2.1}$ ($n = 6$) measured using 2 K bath solution. *C*, representative L267H $I_{Slo2.1}$ recorded from a single oocyte bathed in 104 K solution. V_t was varied from +60 to −120 mV, applied in −10 mV steps. *D*, normalized I–V_t relationship for L267H $I_{Slo2.1}$ ($n = 6$) measured using 104 K bath solution. *E* and *F*, normalized I–V_t relationships for L270W $I_{Slo2.1}$ measured using 2 K ($n = 5$) or 104 K ($n = 5$) bath solution. All data are the mean ± SEM. Arrows to the left of current traces indicate the zero current level. [Colour figure can be viewed at wileyonlinelibrary.com]

mutant channels. Although ion selectivity was altered in most of the constitutively active mutant Slo2.1 channels, there was no significant relationship between $I_{c\text{-}rel}$ and P_{Rb^+}/P_{K^+} (Fig. 7*D*).

M282E Slo2.1 and M354E Slo2.2 channels are not constitutively open

In most K^+ channels, the activation gate that controls ion permeation is formed by the S6 bundle crossing, a criss-crossing of the inner helical transmembrane segments (S6 segments in a Kv channel) near the intracellular end of the inner pore (Doyle *et al.* 1998). The ion conduction pathway is closed when the S6 bundle crossing forms an aperture that is too narrow to allow passive flux of hydrated K^+ ions. In Kv channels, the aperture is widened by electromechanical coupling of the voltage sensor to a splaying of the S6 segments (Long *et al.* 2005). However, replacement of specific hydrophobic S6 residues that line the inner pore with a charged residue

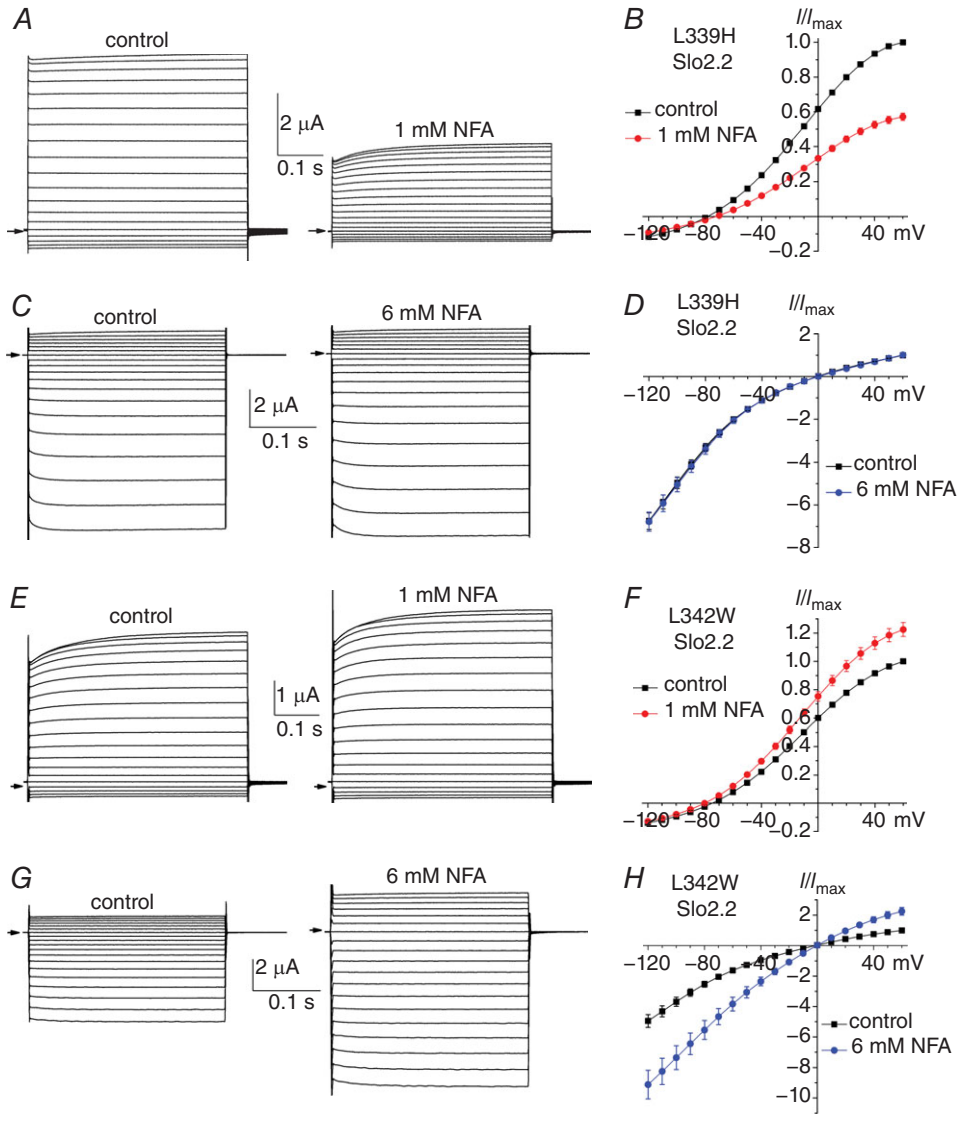

Figure 6. L339H and L342W Slo2.2 channels are constitutively open under control conditions
A and *B*, representative L339H Slo2.2 currents (*A*) and normalized I–V_t relationships (*B*) ($n = 10$) recorded under control conditions (2 K solution) and after treatment with 1 mM NFA. *C* and *D*, representative L339H Slo2.2 currents (*C*) and normalized I–V_t relationships (*D*) ($n = 7$) recorded under control conditions (104 K solution) and after treatment with 6 mM NFA. *E* and *F*, representative L342W Slo2.2 currents (*E*) and normalized I–V_t relationships (*F*) ($n = 11$) recorded under control conditions (2 K solution) and after treatment with 1 mM NFA. *G* and *H*, representative L342W Slo2.2 currents (*G*) and normalized I–V_t relationships (*H*) ($n = 7$) recorded under control conditions (104 K solution) and after treatment with 6 mM NFA. All data are the mean ± SEM. Arrows to the left of current traces indicate the zero current level. [Colour figure can be viewed at wileyonlinelibrary.com]

can fully open the channel in the absence of voltage sensor activation. Examples include P407D in Shaker channels (Hackos *et al.* 2002), as well as A653R(K,E,D) or F656R in hERG1 channels (Fernandez *et al.* 2004, Brown *et al.* 2008). A cryo-EM structure of the chicken Slo2.2 channel obtained in the absence of Na^+ found that the S6 segments are closest to one another at Met333 to constrict the inner pore to a diameter estimated by modelling to be < 4 Å (Hite *et al.* 2015). If indeed the Met residues from all four Slo2 subunits are in sufficiently close proximity to close the ion permeation pathway, then replacement of Met with a charged amino acid should induce constitutive channel opening by electrostatic repulsion. Human Slo2.1 and Slo2.2 channel subunits contain a Met in the same position in the S6 segment as Met333 in chicken Slo2.2. We substituted the native Met residue in Slo2.1 and Slo2.2 channels with Glu, a negatively-charged residue with similar mass and accessible surface area as Met. By contrast to the prediction that the S6 bundle crossing closes the channel, the biophysical properties of both M282E Slo2.1 and M354E Slo2.2 channels were similar to WT channels.

M282E $I_{Slo2.1}$ was undetectable under control conditions but was markedly increased by application of 1 mM NFA (Fig. 8*A* and *B*). Moreover, the EC_{50} for activation of M282E Slo2.1 by NFA was 2.2 ± 0.05 mM (Fig. 8*C* and *D*) ($n = 7$), similar (Dai *et al.* 2010, Garg and Sanguinetti, 2012) or identical (Suzuki *et al.* 2016) to the EC_{50} for NFA determined previously for WT Slo2.1 channels. The conductance of M354E Slo2.2 channels was detectable under basal conditions, similar to WT Slo2.2 channels (Garg and Sanguinetti, 2012), although it was markedly enhanced by NFA (Fig. 9*A* and *B*) with an EC_{50} of 2.7 ± 0.13 mM ($n = 12$) (Fig. 9*C* and *D*). $I_{c\text{-rel}}$ of M354E $I_{Slo2.2}$ in the absence of NFA was 0.05 ± 0.001 (Fig. 9*D*). These properties are almost identical to WT Slo2.2 channels ($I_{c\text{-rel}} = 0.06$; NFA $EC_{50} = 2.7$ mM) (Garg and Sanguinetti, 2012). The onset of activation for both WT and M354E $I_{Slo2.2}$ was biexponential; however, M354E Slo2.2 channels activated more slowly ($\tau_{fast} = 77 \pm 4$ ms, $\tau_{slow} = 310 \pm 16$ ms at +40 mV, $n = 17$) compared to WT Slo2.2 channels ($\tau_{fast} = 16 \pm 0.6$ ms, $\tau_{slow} = 50 \pm 1.5$ ms at +40 mV, $n = 11$) in the presence of 3 mM NFA. It is notable that the onset of Slo2.2 channel currents, when activated with saturating concentrations of NFA, remains quite slow compared to fully activated Slo2.1 channel currents. This finding indicates that the gating mechanisms of Slo2.1 and 2.2 channels are not the same. In summary, replacement of a key Met residue in the S6 segment with a charged Glu residue did not induce constitutive channel opening or enhance the sensitivity of Slo2 channels to activation by NFA. Thus, similar to their corresponding WT channels, M282E Slo2.1 and M354E Slo2.2 channels are stabilized in a closed state. These functional findings argue against the cryo-EM structure based hypothesis that a narrowing of the aperture formed by the S6 bundle crossing is the predominant mechanism of Slo2 channel closure.

Discussion

Under normal physiological conditions, Slo2 channels are predominantly in a closed state but are readily activated

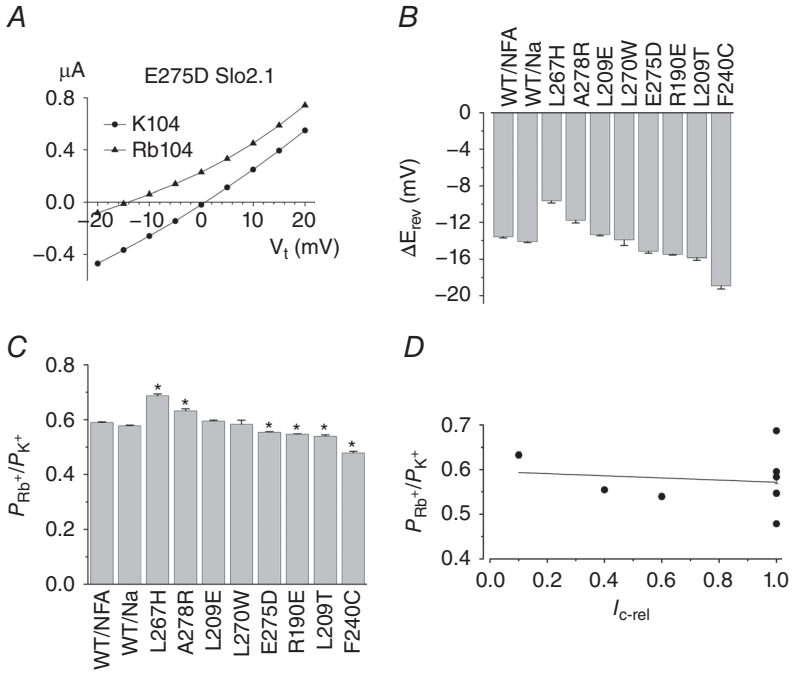

Figure 7. K^+ selectivity of constitutively active Slo2.1 channels
A, plot of peak $I_{Slo2.1}$ *vs.* V_t for E275D Slo2.1 mutant channels in a single oocyte bathed in a solution containing 104 mM KCl or RbCl. *B*, plot of the difference in reversal potential (ΔE_{rev}) determined in oocytes bathed in a solution containing either 104 mM KCl or RbCl ($n = 7$–13). *C*, relative permeability of Rb^+ compared to K^+ (P_{Rb^+}/P_{K^+}) for WT channels, activated with 1 mM NFA or by intracellular Na^+ loading, and constitutively active mutant channels as indicated. $^*P < 0.001$ compared to WT channels activated by NFA. All data are the mean ± SEM. *D*, lack of correlation between P_{Rb^+}/P_{K^+} and $I_{c\text{-rel}}$ for constitutively active mutant Slo2.1 channels (adjusted $r^2 = 0.017$).

in response to an increase in $[Na^+]_i$. The structural basis of low ion permeation under basal conditions and the gating mechanism underlying Na^+-activation of Slo2 channels are not well understood, especially because functional studies of gating are inconsistent with the gating mechanism suggested by the only available Slo2 channel structure (Hite *et al.* 2015). In our previous functional studies of Slo2.1 channels (Garg *et al.* 2013, Suzuki *et al.* 2016), we concluded that the SF performs as the activation gate. SF gating was previously proposed for several other K^+ channels, including Slo1 (Chen and Aldrich, 2011), $K_{Ca}3.1$ (Klein *et al.* 2007, Garneau *et al.* 2014) and $K_{Ca}2$ (Jenkins *et al.* 2011). However, a cryo-EM structure of the chicken Slo2.2 channel showed that the S6 bundle crossing forms a narrow aperture near Met333 sufficient to close the ion permeation pathway (Hite *et al.* 2015), indicating that this structure is the activation gate. Although both the SF and the S6 bundle crossing, acting together or independently, could gate ion permeation, the goal of the present study was to further probe the structural basis of Slo2 channel gating by functional analysis of human Slo2.1 and Slo2.2 channels harbouring mutations of key residues in the S6 segments.

We first explored the possibility that Slo2 channels might be stabilized in a closed state by a hydrophobic barrier located deep within the inner pore, near the SF. This mode of channel closure, referred to as hydrophobic gating was observed during MD simulations of the Kv1.2 channel

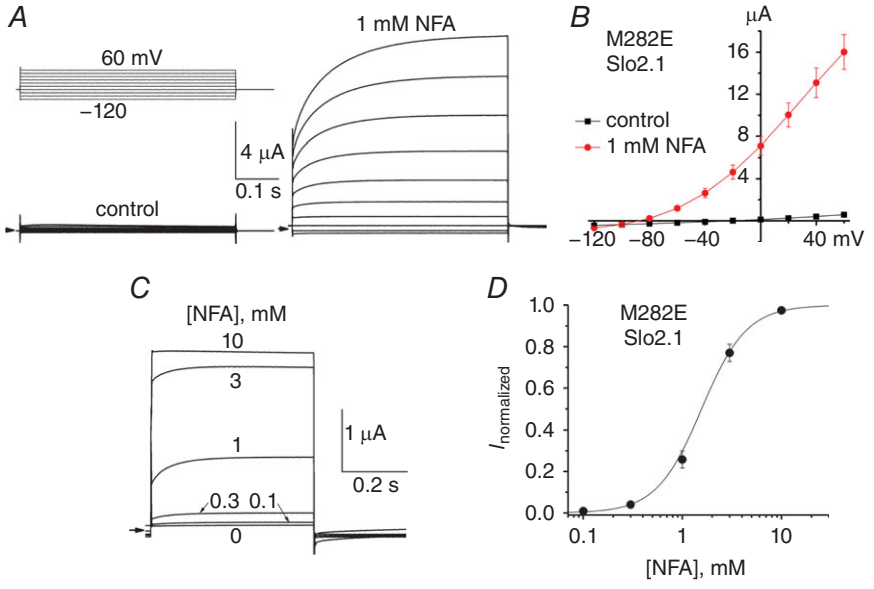

Figure 8. M282E Slo2.1 channels are closed under control conditions
A, representative currents recorded under indicated conditions. *B*, I–V_t relationship for M282E $I_{Slo2.1}$ under basal conditions and after treatment of oocytes with 1 mM NFA ($n = 13$). *C*, peak currents recorded at a V_t of 0 mV in the presence of indicated [NFA]. *D*, [NFA]–response relationship for peak current at a V_t of 0 mV. Data were fitted with a logistic equation (smooth curve). $EC_{50} = 1.74 \pm 0.19$ mM; $n_H = 2.2 \pm 0.05$ ($n = 7$). All data are the mean ± SEM. Arrows to the left of current traces indicate the zero current level. [Colour figure can be viewed at wileyonlinelibrary.com]

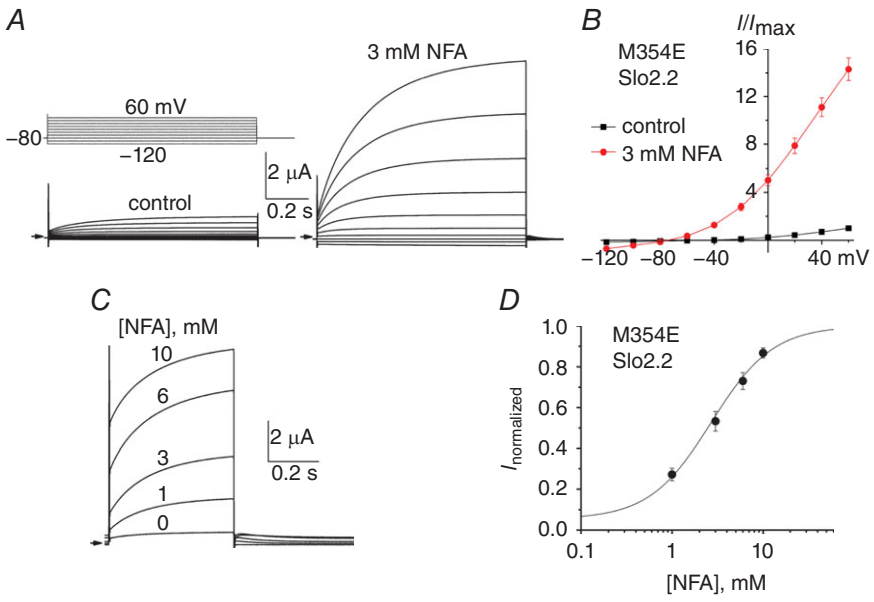

Figure 9. M354E Slo2.2 channels are closed under control conditions
A, representative currents recorded under indicated conditions. *B*, I–V_t relationship for M354E $I_{Slo2.2}$ under basal conditions and after treatment of oocytes with 3 mM NFA ($n = 12$). *C*, peak currents recorded at a V_t of 0 mV in the presence of indicated [NFA]. *D*, [NFA]–response relationship for $I_{Slo2.2}$ at 0 mV. Data were fitted with a logistic equation (smooth curve). $EC_{50} = 2.69 \pm 0.13$ mM; $n_H = 1.3 \pm 0.1$ ($n = 12$). All data are the mean ± SEM. Arrows to the left of current traces indicate the zero current level. [Colour figure can be viewed at wileyonlinelibrary.com]

pore domain (Jensen *et al.* 2010). Dewetting and collapse of the hydrophobic inner pore of Kv1.2 was accelerated at more negative voltages and mediated by a hydrophobic seal formed by Ile402 residues located in each of the four S6 segments (Jensen *et al.* 2010). Curiously, the fastest inner pore closure was at 0 mV, although this was not observed in MD simulations using the full-length channel. Hydrophobic gating has also been proposed for other K^+ channels that have a low open probability under basal condition, including MthK (Ye *et al.* 2010), KcsA and the K2P channel TWIK-1 (Aryal *et al.* 2015). Hydrophobic gating in TWIK-1 channels was mediated by Leu146 in TM2 and Leu261 in TM4, located 5–10 Å below the SF and, as predicted for a hydrophobic gating mechanism, mutation of these residues to a polar residue (Asn) induced constitutive channel activity (Aryal *et al.* 2014). The same region of the inner pore in the chicken Slo2.2 channel is also lined by two hydrophobic Leu residues in each of the four inner helices (S6 segments). In human Slo2.1, these residues are Leu267 and Leu270 (Fig. 1) . Based on sequence alignment of S6 segments, Leu270 in Slo2.1 is homologous to the residue in Kv1.2 (Ile402) implicated in hydrophobic gating. Similar to the approach used to study hydrophobic gating in TWIK-1 channels (Aryal *et al.* 2014), we mutated Leu267 and Leu270 to the isosteric but polar Asn and found that L267N and L267N/L270N (and not L270N alone) greatly stabilized channels in an open state. These findings are consistent with Leu267 having a dominant role in hydrophobic gating of Slo2.1 channels. Leu267 and Leu270 in human Slo2.1 is the equivalent of Leu318 and Leu321 in chicken Slo2.2. In the chicken Slo2.2 structure, the distance between Leu321 C_β residues or Leu318 C_β residues in diagonal subunits is 20–22 Å. Dewetting of the inner pore mediated by these Leu residues could only occur if adjacent S6 segments moved closer to one another. In MD simulations of the Kv1.2 pore domain, the distance between Ile402 C_β residues in diagonal subunits decreased by two-fold from their initial distance of ∼15 Å during the dewetting process associated with complete closure of the upper pore cavity (Jensen *et al.* 2010).

The functional studies reported here are in agreement with previous studies suggesting that, under normal physiological conditions, Slo2 channels are stabilized in a closed state by a mechanism other than constriction of the inner pore at the S6 bundle crossing. Three key findings are most relevant. First, replacement of Met282 in Slo2.1 or Met354 in Slo2.2 with Glu did not induce constitutive channel activity. If the S6 Met residues were sufficiently close to constrict the inner pore and prevent ion permeation (i.e. close the channel), then electrostatic repulsion between the negatively-charged Glu residues was predicted to open the channels. Instead, these mutant channels were stabilized in a closed state similar to WT channels. Second, we previously reported that, in Slo2.1 channels, neutralization of the S6 residue Glu275 by mutation to Ala stabilized channels in a closed state. E275A Slo2.1 channels could not be activated by elevated $[Na^+]_i$ or by application of high concentrations of NFA. However, intragenic rescue of E275A channel function was achieved by specific second site mutations (A278R or Y279E) that inserted a charged residue into a position one helical turn below the introduced Ala275 (Garg *et al.* 2013). These findings suggest that Glu275 maintains the mid-region of the inner pore in a dilated and wetted state, and also that replacement with Ala facilitates a dewetting that constricts a more extensive region of the inner pore and fully stabilizes the channel in a closed state. Dramatic changes in the open probability of other channels have been observed with mutations in residues homologous to Glu275 in Slo2.1. Glu92 is located in the inner helix (TM2) of MthK in a position equivalent to Glu275 of Slo2.1 and neutralization of Glu92 (E92A/Q) stabilizes channels in a closed state (Parfenova *et al.* 2006). Pro475 in Shaker is equivalent to Glu275 in Slo2.1, and mutation to a charged residue (P475D) induces voltage independent constitutive channel opening (Hackos *et al.* 2002). Third, mutations introduced into regions of the PH, S5 and S6 segments in close proximity to the SF stabilize the open state of Slo2.1 channels. Examples include L267H, L267E, L267N/L270N and L270W in S6, as well as F240C in the PH/SF junction (Garg *et al.* 2013) and L209E in the S5 segment (Suzuki *et al.* 2016). It is notable that Leu209 in S5 makes hydrophobic contact with Phe240 and Leu270 contacts both Leu209 and Phe240 (Fig. 1). Together, these findings are consistent with the notion that ion permeation is gated near the upper region of the inner pore and not at the S6 bundle crossing. When the experimental results of the present and previous studies are considered, it remains unclear whether Slo2 channel gating is mediated by the SF gate or hydrophobic gating within the inner pore, or a combination of the two mechanisms. Although ion selectivity was altered in six of the eight constitutively active mutant Slo2.1 channels that were characterized, the absence of a significant relationship between $I_{c\text{-}rel}$ and P_{Rb}/P_K does not help us to distinguish between these two gating mechanisms.

Although it is possible that NFA and elevated $[Na^+]_i$ induce different modes of Slo2.1 gating, the two most important findings of the present study do not depend on the method of channel activation. First, several mutations induced high constitutive channel activity independent of the presence of an activator, including L267H, L270W, L267N and L267N/L270N in Slo2.1, as well as L339H and L342W in Slo2.2. Second, M282E Slo2.1 and M354E Slo2.2 channels have an extremely low open probability in the absence of activators. Together, these findings provide compelling support for the hypothesis that the S6 bundle crossing is not the primary activation gate in Slo2 channels.

Slo2 channels are primarily ligand-gated and exhibit only weak voltage-dependent gating that is not dependent on intramembrane displacement of charges in the voltage sensor because combined neutralization of all the charged residues within the S4 segments of Slo2.1 (K174, E178, D183, R186, H175 and H185) did not appreciably alter the *G–V* relationship (Dai *et al.* 2010). The structure of the chicken Slo2.2 channel indicates that both the cytoplasmic C-terminal gating ring and the S6 bundle crossing are in a closed configuration (Hite *et al.* 2015). This structure was determined in the absence of Na^+ and phosphatidylinositol 4,5-biphosphate. Phosphatidylinositol 4,5-biphosphate increases the amplitude of both Slo2.1 and Slo2.2 channels and this mode of regulation required the Lys residue located one helical turn below the critical Met residue (Met282 in human Slo2.1) in the S6 domain (de los Angeles Tejada *et al.* 2012). How Slo2 channels are activated by binding of Na^+ to the RCK domains of the gating ring is not well understood, although it has been suggested that outward expansion of the gating ring could open the pore either by direct linkage to the S6 domains (causing an outward splaying of the S6 bundle crossing) or by the large protein–protein interface between the RCK1 N-lobes of the gating ring and the S4/S5 transmembrane segments (Hite *et al.* 2015). Analyses of mutant Slo2 channels do not appear to be compatible with this structure-based gating model. The open probability of Slo2.1 channels can be drastically altered by point mutations of Leu267 and Leu270 in S6, Leu209 in S5, and Phe240 in the PH. These residues are in close proximity to one another and near the SF. These functional data are more consistent with the notion that ion permeation in Slo2 channels is predominantly controlled by SF gating or hydrophobic gating of the upper region of the inner pore and not by an S6 bundle crossing gate.

References

Aryal P, Abd-Wahab F, Bucci G, Sansom MS & Tucker SJ (2014). A hydrophobic barrier deep within the inner pore of the TWIK-1 K2P potassium channel. *Nat Commun* **5**, 4377.

Aryal P, Sansom MS & Tucker SJ (2015). Hydrophobic gating in ion channels. *J Mol Biol* **427**, 121–130.

Barcia G, Fleming MR, Deligniere A, Gazula VR, Brown MR, Langouet M, Chen H, Kronengold J, Abhyankar A, Cilio R, Nitschke P, Kaminska A, Boddaert N, Casanova JL, Desguerre I, Munnich A, Dulac O, Kaczmarek LK, Colleaux L & Nabbout R (2012). De novo gain-of-function KCNT1 channel mutations cause malignant migrating partial seizures of infancy. *Nat Genet* **44**, 1255–1259.

Bhattacharjee A, Gan L & Kaczmarek LK (2002). Localization of the Slack potassium channel in the rat central nervous system. *J Comp Neurol* **454**, 241–254.

Bhattacharjee A, Joiner WJ, Wu M, Yang Y, Sigworth FJ & Kaczmarek LK (2003). Slick (Slo2.1), a rapidly-gating sodium-activated potassium channel inhibited by ATP. *J Neurosci* **23**, 11681–11691.

Bhattacharjee A, von Hehn CA, Mei X & Kaczmarek LK (2005). Localization of the Na^+-activated K^+ channel Slick in the rat central nervous system. *J Comp Neurol* **484**, 80–92.

Blatz AL & Magleby KL (1984). Ion conductance and selectivity of single calcium-activated potassium channels in cultured rat muscle. *J Gen Physiol* **84**, 1–23.

Brown S, Sonntag DP & Sanguinetti MC (2008). A highly conserved alanine in the S6 domain of the hERG1 K^+ channel is required for normal gating. *Cell Physiol Biochem* **22**, 601–610.

Bruening-Wright A, Lee WS, Adelman JP & Maylie J (2007). Evidence for a deep pore activation gate in small conductance Ca^{2+}-activated K^+ channels. *J Gen Physiol* **130**, 601–610.

Chen X & Aldrich RW (2011). Charge substitution for a deep-pore residue reveals structural dynamics during BK channel gating. *J Gen Physiol* **138**, 137–154.

Dai L, Garg V & Sanguinetti MC (2010). Activation of Slo2.1 channels by niflumic acid. *J Gen Physiol* **135**, 275–295.

de los Angeles Tejada M, Jensen LJ & Klaerke DA (2012). PIP_2 modulation of Slick and Slack K^+ channels. *Biochem Biophys Res Commun* **424**, 208–213.

Doyle DA, Morais Cabral J, Pfuetzner RA, Kuo A, Gulbis JM, Cohen SL, Chait BT & MacKinnon R (1998). The structure of the potassium channel: molecular basis of K^+ conduction and selectivity. *Science* **280**, 69–77.

Fernandez D, Ghanta A, Kauffman GW & Sanguinetti MC (2004). Physicochemical features of the hERG channel drug binding site. *J Biol Chem* **279**, 10120–10127.

Gao SB, Wu Y, Lu CX, Guo ZH, Li CH & Ding JP (2008). Slack and Slick K_{Na} channels are required for the depolarizing afterpotential of acutely isolated, medium diameter rat dorsal root ganglion neurons. *Acta Pharmacol Sin* **29**, 899–905.

Garg P, Gardner A, Garg V & Sanguinetti MC (2013). Structural basis of ion permeation gating in Slo2.1 K^+ channels. *J Gen Physiol* **142**, 523–542.

Garg P & Sanguinetti MC (2012). Structure-activity relationship of fenamates as Slo2.1 channel activators. *Mol Pharmacol* **82**, 795–802.

Garneau L, Klein H, Banderali U, Longpre-Lauzon A, Parent L & Sauve R (2009). Hydrophobic interactions as key determinants to the KCa3.1 channel closed configuration. An analysis of KCa3.1 mutants constitutively active in zero Ca^{2+}. *J Biol Chem* **284**, 389–403.

Garneau L, Klein H, Lavoie MF, Brochiero E, Parent L & Sauve R (2014). Aromatic-aromatic interactions between residues in KCa3.1 pore helix and S5 transmembrane segment control the channel gating process. *J Gen Physiol* **143**, 289–307.

Goldman DE (1943). Potential, impedance, and rectification in membranes. *J Gen Physiol* **27**, 37–60.

Grissmer S, Nguyen AN & Cahalan MD (1993). Calcium-activated potassium channels in resting and activated human T lymphocytes. Expression levels, calcium dependence, ion selectivity, and pharmacology. *J Gen Physiol* **102**, 601–630.

Grundy D (2015). Principles and standards for reporting animal experiments in The Journal of Physiology and Experimental Physiology. *J Physiol* **593**, 2547–2549.

Hackos DH, Chang TH & Swartz KJ (2002). Scanning the intracellular S6 activation gate in the shaker K^+ channel. *J Gen Physiol* **119**, 521–532.

Hage TA & Salkoff L (2012). Sodium-activated potassium channels are functionally coupled to persistent sodium currents. *J Neurosci* **32**, 2714–2721.

Heron SE, Smith KR, Bahlo M, Nobili L, Kahana E, Licchetta L, Oliver KL, Mazarib A, Afawi Z, Korczyn A, Plazzi G, Petrou S, Berkovic SF, Scheffer IE & Dibbens LM (2012). Missense mutations in the sodium-gated potassium channel gene KCNT1 cause severe autosomal dominant nocturnal frontal lobe epilepsy. *Nat Genet* **44**, 1188–1190.

Hite RK, Yuan P, Li Z, Hsuing Y, Walz T & MacKinnon R (2015). Cryo-electron microscopy structure of the Slo2.2 Na^+-activated K^+ channel. *Nature* **527**, 198–203.

Hodgkin AL & Katz B (1949). The effects of sodium on the electrical activity of the giant axon of the squid. *J Physiol (Lond)* **108**, 37–77.

Jenkins DP, Strobaek D, Hougaard C, Jensen ML, Hummel R, Sorensen US, Christophersen P & Wulff H (2011). Negative gating modulation by (R)-N-(benzimidazol-2-yl)-1,2, 3,4-tetrahydro-1-naphthylamine (NS8593) depends on residues in the inner pore vestibule: pharmacological evidence of deep-pore gating of $K_{Ca}2$ channels. *Mol Pharmacol* **79**, 899–909.

Jensen MO, Borhani DW, Lindorff-Larsen K, Maragakis P, Jogini V, Eastwood MP, Dror RO & Shaw DE (2010). Principles of conduction and hydrophobic gating in K^+ channels. *Proc Natl Acad Sci USA* **107**, 5833–5838.

Kameyama M, Kakei M & Sato R (1984). Intracellular Na^+ activates a K^+ channel in mammalian cardiac cells. *Nature* **309**, 354–356.

Klein H, Garneau L, Banderali U, Simoes M, Parent L & Sauve R (2007). Structural determinants of the closed KCa3.1 channel pore in relation to channel gating: results from a substituted cysteine accessibility analysis. *J Gen Physiol* **129**, 299–315.

Koehler J, Woetzel N, Staritzbichler R, Sanders CR & Meiler J (2009). A unified hydrophobicity scale for multispan membrane proteins. *Proteins* **76**, 13–29.

Krieger E, Joo K, Lee J, Raman S, Thompson J, Tyka M, Baker D & Karplus K (2009). Improving physical realism, stereochemistry, and side-chain accuracy in homology modeling: Four approaches that performed well in CASP8. *Proteins* **77** (Suppl 9), 114–122.

Krieger E, Koraimann G & Vriend G (2002). Increasing the precision of comparative models with YASARA NOVA – a self-parameterizing force field. *Proteins* **47**, 393–402.

Long SB, Campbell EB & Mackinnon R (2005). Voltage sensor of Kv1.2: structural basis of electromechanical coupling. *Science* **309**, 903–908.

Lu R, Bausch AE, Kallenborn-Gerhardt W, Stoetzer C, Debruin N, Ruth P, Geisslinger G, Leffler A, Lukowski R & Schmidtko A (2015). Slack channels expressed in sensory neurons control neuropathic pain in mice. *J Neurosci* **35**, 1125–1135.

Martinez-Espinosa PL, Wu J, Yang C, Gonzalez-Perez V, Zhou H, Liang H, Xia XM & Lingle CJ (2015). Knockout of Slo2.2 enhances itch, abolishes K_{Na} current, and increases action potential firing frequency in DRG neurons. *Elife* **4**.

Parfenova LV, Crane BM & Rothberg BS (2006). Modulation of MthK potassium channel activity at the intracellular entrance to the pore. *J Biol Chem* **281**, 21131–21138.

Piechotta PL, Rapedius M, Stansfeld PJ, Bollepalli MK, Ehrlich G, Andres-Enguix I, Fritzenschaft H, Decher N, Sansom MS, Tucker SJ & Baukrowitz T (2011). The pore structure and gating mechanism of K2P channels. *EMBO J* **30**, 3607–3619.

Posson DJ, McCoy JG & Nimigean CM (2013). The voltage-dependent gate in MthK potassium channels is located at the selectivity filter. *Nat Struct Mol Biol* **20**, 159–166.

Punta M & Maritan A (2003). A knowledge-based scale for amino acid membrane propensity. *Proteins* **50**, 114–121.

Richards FM (1977). Areas, volumes, packing and protein structure. *Annu Rev Biophys Bioeng* **6**, 151–176.

Rizzi S, Knaus HG & Schwarzer C (2016). Differential distribution of the sodium-activated potassium channels slick and slack in mouse brain. *J Comp Neurol* **524**, 2093–2116.

Schreibmayer W, Lester HA & Dascal N (1994). Voltage clamping of *Xenopus laevis* oocytes utilizing agarose-cushion electrodes. *Pflügers Arch* **426**, 453–458.

Stühmer W (1992). Electrophysiological recording from *Xenopus* oocytes. *Methods Enzymol* **207**, 319–339.

Suzuki T, Hansen A & Sanguinetti MC (2016). Hydrophobic interactions between the S5 segment and the pore helix stabilizes the closed state of Slo2.1 potassium channels. *Biochim Biophys Acta* **1858**, 783–792.

Thompson J & Begenisich T (2012). Selectivity filter gating in large-conductance Ca^{2+}-activated K^+ channels. *J Gen Physiol* **139**, 235–244.

Thomson SJ, Hansen A & Sanguinetti MC (2015). Identification of the intracellular Na^+ sensor in Slo2.1 potassium channels. *J Biol Chem* **290**, 14528–14535.

Vanderver A, Simons C, Schmidt JL, Pearl PL, Bloom M, Lavenstein B, Miller D, Grimmond SM & Taft RJ (2014). Identification of a novel de novo p.Phe932Ile KCNT1 mutation in a patient with leukoencephalopathy and severe epilepsy. *Pediatr Neurol* **50**, 112–114.

Wang W, Black SS, Edwards MD, Miller S, Morrison EL, Bartlett W, Dong C, Naismith JH & Booth IR (2008). The structure of an open form of an *E. coli* mechanosensitive channel at 3.45 Å resolution. *Science* **321**, 1179–1183.

White MM & Aylwin M (1990). Niflumic and flufenamic acids are potent reversible blockers of Ca^{2+}-activated Cl^- channels in *Xenopus* oocytes. *Mol Pharmacol* **37**, 720–724.

Wilkens CM & Aldrich RW (2006). State-independent block of BK channels by an intracellular quaternary ammonium. *J Gen Physiol* **128**, 347–364.

Yang B, Desai R & Kaczmarek LK (2007). Slack and Slick K_{Na} channels regulate the accuracy of timing of auditory neurons. *J Neurosci* **27**, 2617–2627.

Ye S, Li Y & Jiang Y (2010). Novel insights into K^+ selectivity from high-resolution structures of an open K^+ channel pore. *Nat Struct Mol Biol* **17**, 1019–1023.

Yuan A, Santi CM, Wei A, Wang ZW, Pollak K, Nonet M, Kaczmarek L, Crowder CM & Salkoff L (2003). The sodium-activated potassium channel is encoded by a member of the Slo gene family. *Neuron* **37**, 765–773.

Zhang Z, Rosenhouse-Dantsker A, Tang QY, Noskov S & Logothetis DE (2010). The RCK2 domain uses a coordination site present in Kir channels to confer sodium sensitivity to Slo2.2 channels. *J Neurosci* **30**, 7554–7562.

Zilberberg N, Ilan N & Goldstein SA (2001). KCNKO: opening and closing the 2-P-domain potassium leak channel entails "C-type" gating of the outer pore. *Neuron* **32**, 635–648.

Additional information

Competing interests

The authors declare that they have no competing interests.

Author contributions

MHG and MCS designed the study. MHG, AG and MCS acquired, analysed and interpreted the data. MCS and MHG wrote the manuscript. AH provided molecular biology support. All authors approved the final version of the manuscript and agree to be accountable for all aspects of the work in ensuring that questions related to the accuracy or integrity of any part of the work are appropriately investigated and resolved. All persons designated as authors qualify for authorship, and all those who qualify for authorship are listed.

Funding

This work was supported by a grant from the Nora Eccles Treadwell Foundation.